Neurobiology of Aging 77 (2019) 104–111

Contents lists available at ScienceDirect

Neurobiology of Aging

journal homepage: www.elsevier.com/locate/neuaging

Associations of amygdala volume and shape with transactive response DNA-binding protein 43 (TDP-43) pathology in a community cohort of older adults

Nazanin Makkinejad [a], Julie A. Schneider [b,c,d], Junxiao Yu [a], Sue E. Leurgans [b,d], Aikaterini Kotrotsou [a], Arnold M. Evia [a], David A. Bennett [b,d], Konstantinos Arfanakis [a,b,e,*]

[a] Department of Biomedical Engineering, Illinois Institute of Technology, Chicago, IL, USA
[b] Rush Alzheimer's Disease Center, Rush University Medical Center, Chicago, IL, USA
[c] Department of Pathology, Rush University Medical Center, Chicago, IL, USA
[d] Department of Neurological Sciences, Rush University Medical Center, Chicago, IL, USA
[e] Department of Diagnostic Radiology, Rush University Medical Center, Chicago, IL, USA

ARTICLE INFO

Article history:
Received 10 July 2018
Received in revised form 18 January 2019
Accepted 21 January 2019
Available online 31 January 2019

Keywords:
MRI
Ex vivo
Pathology
Amygdala
TDP-43
Alzheimer's
Hippocampal sclerosis
Volume
Shape
Cognitive decline

ABSTRACT

Transactive response DNA-binding protein 43 (TDP-43) pathology is common in old age and is strongly associated with cognitive decline and dementia above and beyond contributions from other neuropathologies. TDP-43 pathology in aging typically originates in the amygdala, a brain region also affected by other age-related neuropathologies such as Alzheimer's pathology. The purpose of this study was two-fold: to determine the independent effects of TDP-43 pathology on the volume, as well as shape, of the amygdala in a community cohort of older adults, and to determine the contribution of amygdala volume to the variance of the rate of cognitive decline after accounting for the contributions of neuropathologies and demographics. Cerebral hemispheres from 198 participants of the Rush Memory and Aging Project and the Religious Orders Study were imaged with MRI ex vivo and underwent neuropathologic examination. Measures of amygdala volume and shape were extracted for all participants. Regression models controlling for neuropathologies and demographics showed an independent negative association of TDP-43 with the volume of the amygdala. Shape analysis revealed a unique pattern of amygdala deformation associated with TDP-43 pathology. Finally, mixed-effects models showed that amygdala volume explained an additional portion of the variance of the rate of decline in global cognition, episodic memory, semantic memory, and perceptual speed, above and beyond what was explained by demographics and neuropathologies.

1. Introduction

Transactive response DNA-binding protein 43 (TDP-43) pathology, the primary protein abnormality in the rare, typically presenile, neurodegenerative diseases frontotemporal lobar degeneration and amyotrophic lateral sclerosis (Neumann et al., 2006), is now recognized as a common age-related neuropathology, detected at autopsy in approximately 50% of older persons. TDP-43 pathology has been reported in up to 55% of persons with Alzheimer's disease (AD) pathology (Arai et al., 2009; Tremblay et al., 2011), 60% of persons with Lewy bodies (Arai et al., 2009), 90% of persons with hippocampal sclerosis (Zarow et al., 2012), and in other neurodegenerative diseases (Freeman et al., 2008; Fujishiro et al., 2009; Geser et al., 2008; Lippa et al., 2010; Olivé et al., 2009; Schwab et al., 2008, 2009; Uryu et al., 2013; Wider et al., 2009). Yet, TDP-43 has also been detected in normal older persons (Arnold et al., 2013; Davidson et al., 2011; Geser et al., 2010; Mcaleese et al., 2016; Uchino et al., 2015; Wilson et al., 2013). The effect of TDP-43 pathology on cognition of older adults is devastating. TDP-43 pathology in aging is strongly and independently associated with cognitive decline and increased risk of dementia above and beyond the contributions of other age-related neuropathologies (Josephs, 2010; Nelson et al., 2010; Wilson et al., 2013). Moreover, TDP-43 pathology in aging has been shown to account for nearly as much of the variance of late-life cognitive decline as neurofibrillary

* Corresponding author at: Department of Biomedical Engineering, Illinois Institute of Technology, 3440 South Dearborn St. M-102 Chicago, IL 60616. Tel.: (+312) 567-3864.
E-mail address: arfanakis@iit.edu (K. Arfanakis).

0197-4580/$ – see front matter © 2019 Elsevier Inc. All rights reserved.
https://doi.org/10.1016/j.neurobiolaging.2019.01.022

tangles (hallmark pathology of AD) (Wilson et al., 2013). Thus, TDP-43 pathology is now recognized as a common and deleterious neuropathology of the aging brain.

Deposition of TDP-43 pathology in aging typically begins, and is most commonly seen, in the amygdala. In persons with AD, it was previously shown that TDP-43 pathology is first deposited in the amygdala, followed by the hippocampus and entorhinal cortex, and then the neocortex and other regions (James et al., 2016; Josephs et al., 2014a). In cases with Lewy bodies with no or low tau burden, the amygdala was shown to have TDP-43 inclusions in all TDP-43 positive cases, whereas other regions were less frequently affected by TDP-43 (e.g., the entorhinal cortex, followed by the hippocampus and other cortical regions) (Yokota et al., 2010). In progressive supranuclear palsy, TDP-43 was again found most frequently in the amygdala, followed by hippocampus, entorhinal cortex, and other regions (Koga et al., 2016). In persons with hippocampal sclerosis, TDP-43 inclusions were most frequent in the amygdala compared to other brain regions (Nag et al., 2015). In older adults who were cognitively normal at the time of death, the amygdala was again the most common location for TDP-43 deposition (Arnold et al., 2013). In community-dwelling older adults, the amygdala exhibited TDP-43 inclusions in all individuals with the pathology, and as TDP-43 progressed from the amygdala to the hippocampus or entorhinal cortex and to the neocortex, there was a gradual increase of inclusions in the amygdala (Nag et al., 2018). The above findings suggest that the amygdala is involved early on in the progression of TDP-43 in aging, and is most often affected by TDP-43 pathology compared to any other brain region. Therefore, identifying amygdala abnormalities that are linked to TDP-43 pathology in aging and are detectable by MRI may be of high significance for the development of future strategies for the detection of the pathology.

Little is known about MR-detectable amygdala abnormalities associated with TDP-43 pathology in aging. A single recent MR-volumetry and pathology study on 248 older adults with pathologic diagnosis of AD and 46 controls showed a significant association between lower amygdala volumes and TDP-43 pathology (Josephs et al., 2014b). However, MRI was conducted in vivo, allowing additional pathology to develop between imaging and autopsy, thereby potentially underestimating the effects of pathology on brain MR characteristics. Furthermore, all MRI scans were conducted between 1992–2010, primarily on 1.5 Tesla (T) scanners, suggesting potentially high coefficient of variation for volume measurements in small brain regions such as the amygdala, especially for data collected on older scanners. In addition, although analyses controlled for an extensive list of neurodegenerative pathologies, infarcts were the only vascular pathology controlled for. To our knowledge, there are no reports in the literature on amygdala shape abnormalities associated with TDP-43 pathology in aging. Shape analysis can provide important information on the spatial distribution of atrophy or expansion of a structure that exhibits volume abnormalities and based on the substructures involved and their functional role may aid in understanding the functional outcomes of such volume abnormalities. Finally, no studies on the links between amygdala structural abnormalities and TDP-43 pathology in aging have been conducted in a community cohort.

The purpose of this study was to determine the independent effects of TDP-43 pathology in aging on both the volume and shape of the amygdala, by combining ex vivo MRI and pathology in a large community cohort of older adults. By using ex vivo MRI, no additional pathology developed between imaging and pathologic examination, and frail older adults were not excluded from MRI, thereby eliminating 2 important biases. Clinical 3 T MRI scanners and pulse sequences were used to generate sufficient data quality while enhancing in vivo translation of potential findings. A comprehensive set of age-related neuropathologies was considered in analyses to more accurately delineate the independent effects of TDP-43 pathology in aging. Shape analysis was used in addition to volumetry to extract the unique amygdala deformation pattern associated with TDP-43, which may be more informative than global amygdala volume changes alone. Finally, the contribution of amygdala volume to the variance of the rate of cognitive decline was assessed, after accounting for the contributions of neuropathologies and demographics. This study was conducted in a community cohort to enhance the generalizability of potential findings.

2. Methods

2.1. Study population

Individuals enrolled in 2 longitudinal clinical-pathologic cohort studies of aging, the Rush University Memory and Aging Project (MAP) and the Religious Order Study (ROS) (Bennett et al., 2018), were included in this investigation. Both studies were approved by the institutional review board of Rush University Medical Center. All participants provided written informed consent and signed an anatomical gift act. Annual clinical evaluation including cognitive function testing, medical history, and neurologic examination was performed on all participants. Diagnosis of dementia and AD was based on the criteria of the National Institute of Neurological and Communicative Disorders and Stroke and the Alzheimer Disease and Related Disorders Association (NINCDS/ADRA) (McKhann et al., 1984). Participants who had cognitive impairment but did not meet the criteria for dementia were classified as having mild cognitive impairment (Bennett et al., 2002; Boyle et al., 2006). At the time of these analyses, 3194 MAP/ROS participants had completed the baseline clinical evaluation. Of these, 572 died and 78 withdrew from the study before the ex vivo MRI sub-study began. Of the remaining 2544 persons, 952 died, 816 were autopsied, and 646 had ex vivo MRI. Amygdala segmentation was conducted in the first 208 consecutive cases. Of these 208 persons, 2 did not have TDP-43 pathology data, and 8 failed the subsequent shape analysis procedure. Hence, analyses were performed on the first 198 eligible participants (Table 1).

2.2. Cognitive testing

A battery of 21 cognitive tests was administered to all participants annually. One of the tests, the Mini-Mental State Examination, was used only for descriptive purposes, and a second test, the Complex Ideational Material, was used only for diagnostic purposes. The remaining 19 tests were used to evaluate performance in 5 cognitive domains: 7 tests for episodic memory, 3 for semantic memory, 3 for working memory, 4 for perceptual speed, and 2 for visuospatial ability (Bennett et al., 2018). Raw scores for each test were converted to z-scores, and were averaged across all 19 tests to obtain a composite score of global cognition (Wilson et al., 2003). For each cognitive domain, the z-scores from the corresponding tests were also averaged into a composite score for that cognitive domain (Bennett et al., 2006).

2.3. Brain hemisphere preparation

On a participant's death, an autopsy technician removed the brain, and the cerebrum was separated from the cerebellum and brainstem. The cerebrum was divided into the left and right hemispheres by cutting the corpus callosum, and the hemisphere with more visible pathology was selected for ex vivo MRI and pathologic examination, while the contralateral hemisphere was frozen and stored. The selected hemisphere was immersed in phosphate-buffered 4% formaldehyde solution and refrigerated at

4 °C, within 30 minutes of removal from the skull. Ex vivo MRI was conducted while the hemisphere was immersed in formaldehyde solution with its medial aspect facing the bottom of an MR-compatible container, at room temperature. Gross examination was performed within 2 weeks after ex vivo MRI, followed by histopathologic diagnostic examination by a board-certified neuropathologist (Kotrotsou et al., 2015).

2.4. Ex vivo MRI data acquisition and preprocessing

All imaging data were collected on 3 Tesla MRI scanners (Table 1) using a 2D spin-echo sequence with multiple echo times. Because of the ongoing nature of this study and scanner upgrades, 3 MRI scanners with similar imaging protocols were used for data collection (Dawe et al., 2014). The voxel size was 0.6 × 0.6 × 1.5 mm^3 for all scanners, and only T2-weighted images collected at echo times between 50–58 ms were used in the analysis.

The gray matter of the T2-weighted image volumes from all hemispheres was segmented into 42 cortical and subcortical regions using a published multiatlas approach based on 25 atlases (Kotrotsou et al., 2014), and amygdala segmentation in each hemisphere was further refined using manual corrections (Fig. 1). The volume of the amygdala was calculated for each hemisphere as the product of the number of voxels within the segmented region and the voxel volume. The amygdala volume was then normalized by the participant's height, which has previously been used as a surrogate for total intracranial volume (Dawe et al., 2011; Kotrotsou et al., 2015; Van Petten, 2004).

Because surface alignment is not well defined on shapes with rotational symmetry such as the amygdala (Styner et al., 2003), initial correspondence of amygdala surfaces was established by whole hemisphere registration. More specifically, the image volumes from all hemispheres were rigidly registered to a template using FSL (FMRIB, Oxford, UK) (Smith et al., 2004). The resulting rigid body transforms were then applied to the amygdala masks.

Table 1
Demographic and clinical characteristics of the participants

Characteristics	Total
N	198
Age at death, y (SD)	90 (6)
Male, n (%)	57 (29%)
Education, y (SD)	16 (4)
Years of clinical follow-up, mean (SD)	8 (5)
Median time between last evaluation and death, years (interquartile range)	0.78 (0.4–1.2)
Clinical diagnosis proximate to death, n (%)	
No cognitive impairment	55 (28%)
Mild cognitive impairment	43 (22%)
Dementia	100 (50%)
Global cognition score[a], mean (SD)	−1.1 (1.2)
Episodic memory score[a], mean (SD)	−1.0 (1.4)
Semantic memory score[a], mean (SD)	−1.4 (1.6)
Working memory score[a], mean (SD)	−0.9 (1.1)
Perceptual speed score[a], mean (SD)	−1.3 (1.2)
Visuospatial ability score[a], mean (SD)	−0.7 (1.2)
Mini-mental state examination[a] (MMSE), mean (SD)	19.5 (9.6)
Mini-mental State examination[a] (MMSE), median	23.4
Right hemisphere, n (%)	93 (47%)
Postmortem interval to fixation, hours (SD)	8.6 (6.5)
Postmortem interval to imaging, d (SD)	49.6 (24.0)
MRI scanner, n (%)	
General Electric, 3 Tesla, n (%)	48 (24%)
Participants with TDP-43, n (%)	22 (46%)
Philips, 3 Tesla, n (%)	85 (43%)
Participants with TDP-43, n (%)	27 (32%)
Siemens, 3 Tesla, n (%)	65 (33%)
Participants with TDP-43, n (%)	22 (34%)

[a] Proximate to death.

2.5. Shape analysis

Shape analysis was conducted using the spherical harmonic basis function toolbox SPHARM-PDM (Styner et al., 2006). For each hemisphere, the rigidly transformed amygdala mask from the previous step was smoothed using level set based anti-alias smoothing. A triangulated mesh was generated on the surface of the amygdala mask, and a spherical parameterization was obtained by mapping the mesh to a sphere using an area preserving and distortion minimizing spherical mapping algorithm. SPHARM represents an original surface through a weighted linear combination of spherical harmonic basis functions. The spherical harmonic degree was set at 15. The parameterization was then sampled with icosahedron subdivision at level 10, which formed a triangulated mesh with 1002 vertices on the amygdala surface. The meshes from all hemispheres were spatially aligned using the Procrustes rigid body transformation, were normalized with the participants' height, and were averaged. For each hemisphere, the difference vector from a vertex on the average mesh to the corresponding vertex on the individual hemisphere's mesh was calculated, and the process was repeated for all vertices. Each difference vector was then projected to the normal vector on the corresponding vertex of the average mesh to obtain a signed shape difference of an individual's amygdala from the average. The signed shape differences were used in statistical analysis (see below).

2.6. Neuropathologic evaluation

Following MRI, each hemisphere was sectioned into 1-cm thick coronal slabs. The slabs underwent macroscopic evaluation and dissection of selected tissue blocks, which were embedded in paraffin, cut into sections, and mounted on glass slides. Neuropathologic evaluation was completed by a board-certified neuropathologist blinded to all clinical data and age, and following well-established procedures. A detailed description of neuropathologic evaluation can be found in Kotrotsou et al. (2015). The score assigned to each neuropathology represented the global burden in the hemisphere and not specifically in the amygdala. TDP-43 was rated on 4 levels capturing the staging of the pathology (no inclusions; inclusions in amygdala only; inclusions in amygdala as well as entorhinal cortex or hippocampus CA1; and inclusions in amygdala, entorhinal cortex or hippocampus CA1, and neocortex) (Yu et al., 2015). A composite score of global AD pathology was given for each hemisphere based on plaque and tangle counts in 5 brain regions (Schneider et al., 2007). Hippocampal sclerosis was rated as present or absent (Schneider et al., 2009). Lewy bodies were detected in 6 regions and were rated as present or absent (McKeith et al., 1996; Schneider et al., 2012). Gross infarcts were scored as none, one, or more than one. Microscopic infarcts were detected in a minimum of 9 regions and were scored as none, one, or more than one (Arvanitakis et al., 2011a). Atherosclerosis and arteriolosclerosis were scored as none, mild, moderate, and severe. Cerebral amyloid angiopathy was assessed in 4 regions and was rated as none, mild, moderate, and severe (Arvanitakis et al., 2011b).

2.7. Statistical analysis

The least absolute shrinkage and selection operator (LASSO) approach was employed to investigate the association of amygdala volume (dependent variable), as well as signed shape differences at all vertices of the average mesh (dependent variables), with (independent variables) TDP-43, hippocampal sclerosis, AD pathology, Lewy bodies, arteriolosclerosis, atherosclerosis, gross and microscopic infarcts, and cerebral amyloid angiopathy, while controlling for age at death, sex, years of education, scanner, duration between death and

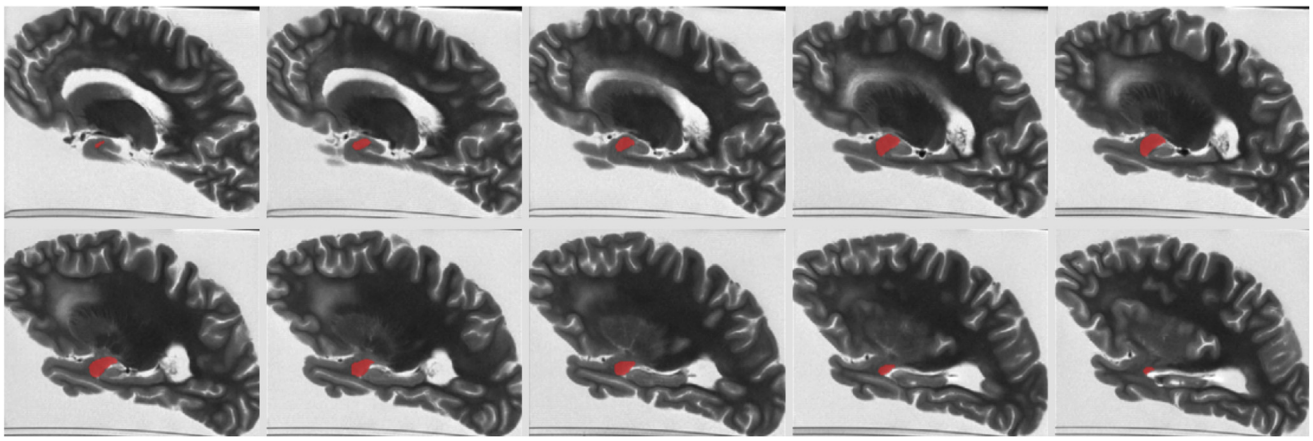

Fig. 1. An example of amygdala segmentation for a cerebral hemisphere of one of the participants.

immersion in formaldehyde solution (postmortem interval to fixation, PMI), and duration between death and ex vivo MRI (postmortem interval to imaging, PMII). LASSO is a penalized regression model, where l_1 regularization is added to the standard multiple linear regression model. The optimal penalty factor was calculated by a leave-one-out cross validation procedure by minimizing the mean squared error and enforcing sparsity in the output model. All models were implemented in R version 3.4.0 (The R Foundation for Statistical Computing). For the signed shape differences, p-values were corrected for multiple comparisons using the false discovery rate approach (Benjamini and Hochberg, 1995). Associations of amygdala volume and signed shape differences with neuropathologies were considered significant at $p < 0.05$. The Shape Population Viewer Toolbox (www.nitrc.org/projects/shapepopviewer/) was used for visualization of shape analysis results.

Two linear mixed-effects models were used to assess the contribution of amygdala volume measured ex vivo to the variance of the rate of decline in global cognition above and beyond what was explained by neuropathologies and demographics. The composite score of global cognition was the longitudinal-dependent variable in both models. The independent variables in the first model were all the neuropathologies, demographics, and covariates listed in the previous paragraph, as well as the interaction of each one of these variables with time since baseline. The independent variables in the second model included those of the first model plus the volume of the amygdala and its interaction with time since baseline. The percent difference in the variance of the rate of decline between the 2 mixed-effects models provided the additional percentage of variance explained by amygdala volume above and beyond what was explained by pathologies and demographics. Both models were implemented in R version 3.4.0 (The R Foundation for Statistical Computing), and the additional variance explained by amygdala volume was considered significant when the interaction term of amygdala volume with time since baseline was statistically significant ($p < 0.05$). The same analysis was repeated for each of the 5 cognitive domains.

3. Results

3.1. Demographic, clinical, and neuropathologic characteristics

Demographic and clinical characteristics of the participants are presented in Table 1, and neuropathologic characteristics are presented in Table 2. When comparing this sample to 464 other participants of the parent studies who had an autopsy after the start of the present work, the present sample had on average 1.2 more years of education ($p < 0.0001$), 0.2 lower global cognition score proximate to death ($p = 0.048$), 0.22 lower working memory score ($p = 0.02$), 0.38 lower visuospatial abilities score ($p < 0.0001$), and more severe atherosclerosis (the 464 individuals were distributed as follows: none = 26%, mild = 52%, moderate = 18%, severe = 5%; compare to the atherosclerosis distribution shown in Table 2) ($p < 0.0001$). No significant differences in amygdala volume were observed across scanners used in this work (ANOVA, $F(2, 195) = 1.16$, $p = 0.32$).

3.2. Associations of amygdala volume and shape with neuropathology

LASSO regression analysis showed a negative correlation of normalized amygdala volume with TDP-43 (model estimate = -31.5 mm^2, $p = 0.0003$), AD pathology (model estimate = -75.0 mm^2, $p < 10^{-4}$), and hippocampal sclerosis (model estimate = -95.4 mm^2, $p = 0.0004$) but not with any other neuropathologies. The independent contributions of TDP-43, AD pathology, and hippocampal sclerosis on the surface of the amygdala are shown before and after false discovery rate correction for multiple comparisons in Fig. 2A and B, respectively. All parts of the amygdala surface with significant associations with neuropathologies showed inward deformation, and are represented with warm colors in Fig. 2. Inward deformations associated with TDP-43 were located in portions of the centromedial, superficial, and laterobasal subdivisions of the amygdala (Fig. 2B) (Amunts et al., 2005). Deformations linked to AD and hippocampal sclerosis were mainly in the superficial and laterobasal subdivisions and were generally more extensive than those linked to TDP-43 (Fig. 2B). Repeating all analyses after removing 2 of the 24 participants with hippocampal sclerosis that were TDP-43 negative, resulted in very similar associations of amygdala volume and shape with neuropathologies as those described above. Also, repeating all analyses in the group of 137 participants with intermediate or high likelihood of AD (according to NIA-Reagan criteria) resulted in very similar associations of amygdala volume and shape with neuropathologies as those described above. In contrast, repeating all analyses in the group of 61 participants with low likelihood or no AD did not result in any significant findings, which may be because of the small size of that group.

3.3. Contribution of amygdala volume to the variance of the rate of cognitive decline

Mixed-effects models revealed that, first, lower amygdala volume was independently associated with faster decline in global cognition (model estimate = $1.8 \cdot 10^{-4}$, $p = 0.009$), episodic memory

Table 2
Neuropathologic characteristics of the participants

Characteristics	Total
NIA-Reagan (Likelihood of AD), n (%)	
High or intermediate likelihood	137 (69%)
Low Likelihood or No AD	61 (31%)
Composite score of global AD pathology, mean (SD)	0.8 (0.6)
Lewy bodies, n (%)	43 (22%)
Hippocampal sclerosis, n (%)	24 (12%)
Gross infarcts, n (%)	93 (47%)
Microscopic infarcts, n (%)	73 (37%)
Atherosclerosis, n (%)	
Severe	23 (12%)
Moderate	53 (27%)
Mild	87 (44%)
None	35 (18%)
Arteriosclerosis, n (%)	
Severe	20 (10%)
Moderate	34 (17%)
Mild	93 (47%)
None	51 (26%)
Cerebral amyloid angiopathy, n (%)	
Severe	19 (10%)
Moderate	51 (26%)
Mild	92 (47%)
None	36 (18%)
TDP-43, n (%)	
Inclusions in amygdala, entorhinal cortex or hippocampus CA1, and neocortex	28 (14%)
Inclusions in amygdala and entorhinal cortex or hippocampus CA1	58 (30%)
Inclusions in amygdala only	41 (21%)
No inclusions	71 (36%)

(model estimate $= 1.7 \cdot 10^{-4}$, $p = 0.027$), semantic memory (model estimate $= 2.4 \cdot 10^{-4}$, $p = 0.0012$), and perceptual speed (model estimate $= 1.8 \cdot 10^{-4}$, $p = 0.029$), controlling for neuropathologies, demographics, and covariates (Table 3). Second, mixed-effects models also revealed that the amygdala volume explained an additional 8.1% of the variance of the rate of decline in global cognition, 5.3% of the variance of the rate of decline in episodic memory, 8.7% in semantic memory, and 3.8% in perceptual speed, above and beyond what was explained by neuropathologies and demographics (Table 3).

4. Discussion

The present study investigated the association of TDP-43 pathology in aging with the volume and shape of the amygdala by combining ex vivo MRI and pathology on a community cohort of older adults. TDP-43 pathology in aging was found to be negatively correlated with the volume of the amygdala, independent of the effects of other neuropathologies. TDP-43 pathology in aging was also associated with a unique spatial pattern of inward deformation of the amygdala surface that was different than the patterns linked to AD pathology and hippocampal sclerosis. Finally, the volume of the amygdala was found to explain an additional portion of the variance of the rate of decline in global cognition, episodic memory, semantic memory, and perceptual speed, above and beyond what was explained by neuropathologies and demographics.

The finding showing an independent negative association of amygdala volume with TDP-43 pathology in aging is in general agreement with a recent report in persons with a pathologic diagnosis of AD (Josephs et al., 2014b). The present study extended the previous work to a community cohort with a range of cognitive function, enhancing generalization of the findings. In addition, the present study combined neuropathology and ex vivo MRI, instead of in vivo MRI, eliminating the possibility of additional pathology developing between imaging and autopsy, and thereby avoiding underestimation of the effects of pathology detected by MRI. Furthermore, use of ex vivo, instead of in vivo MRI ensured that participation in the present study was independent of frailty level. In addition, a more comprehensive set of neurodegenerative and vascular neuropathologies, as well as demographics (Tang et al., 2017), was controlled for in the analyses of the present study. Thus, the current methodology extended previous work and more accurately delineated the independent effects of TDP-43 pathology on the volume of the amygdala in community-dwelling older adults.

Undoubtedly, investigating the volume of the amygdala alone cannot reveal the subtle differences between the effects of TDP-43 and other neuropathologies on amygdala structure. Shape analysis addressed this limitation and mapped the independent spatial pattern of amygdala deformation associated with TDP-43 pathology. Although the spatial extent of the TDP-43–related inward deformation of the amygdala surface was spatially more limited compared to that linked to AD pathology and hippocampal sclerosis, the shape abnormalities associated with TDP-43 involved the centromedial, superficial, and laterobasal subdivisions of the amygdala, whereas those associated with AD pathology and hippocampal sclerosis involved mainly the superficial and laterobasal subdivisions (Amunts et al., 2005). To our knowledge this is the first study mapping the independent spatial patterns of amygdala deformation associated with TDP-43 pathology and hippocampal sclerosis. Our finding that AD pathology is associated with superficial and laterobasal inward deformation with relative sparing of the centromedial subdivision is in general agreement with previous in vivo MRI work on the association of clinical AD diagnosis with the shape of the amygdala (Miller et al., 2015; Qiu et al., 2009; Tang et al., 2015, 2014). This agreement serves as confirmation that ex vivo MRI can provide similar information on amygdala shape as that originating from in vivo MRI, increasing confidence on the novel TDP-43 and hippocampal sclerosis patterns generated here. In addition, our spatial pattern of AD-related amygdala deformation is in general agreement with neuropathologic reports on the distribution of neurofibrillary tangles and neuritic plaques in the amygdala (Kromer Vogt et al., 1990). On the other hand, a study by Cavedo et al. (2011), on 19 patients with AD and 19 healthy controls, showed AD-related inward deformation even in the centromedial subdivision, while in the present work, centromedial deformation was only associated with TDP-43. Since TDP-43 pathology is often present in persons with AD, and since the study by Cavedo et al. (2011) was based on clinical diagnosis of AD, the centromedial deformation seen in that previous study may have been because of undetected comorbid TDP-43.

The results of shape analysis may provide important insight into the functional outcomes of TDP-43 pathology in aging. Inward deformations of the laterobasal and superficial subdivisions of the amygdala were independently associated with TDP-43, as well as with AD and hippocampal sclerosis. The laterobasal subdivision is the main hub connecting the amygdala to the hippocampus, entorhinal cortex (Pikkarainen et al., 1999; Pitkänen et al., 2002), thalamus, and association sensory cortex (Price, 2003) and includes nuclei that are involved in emotional processing and storage of emotional memories (LeDoux and Schiller, 2009). The finding of laterobasal atrophy associated with TDP-43, AD, and hippocampal sclerosis is in agreement with memory deficits associated with all 3 neuropathologies (Wilson et al., 2013). The superficial subdivision of the amygdala has connections to the olfactory bulb and accessory olfactory bulb (Price, 2003). The finding of atrophy in the superficial subdivision associated with AD pathology may be related to the anosmia seen in AD (Doty, 2017). Although no studies have yet linked TDP-43 pathology in aging and hippocampal sclerosis to olfactory abnormalities, recently, TDP-43 pathology has been detected in the olfactory bulb of patients with AD (Josephs and Dickson, 2016), and TDP-43 has been linked to olfactory dysfunction in patients with amyotrophic lateral sclerosis (Takeda et al.,

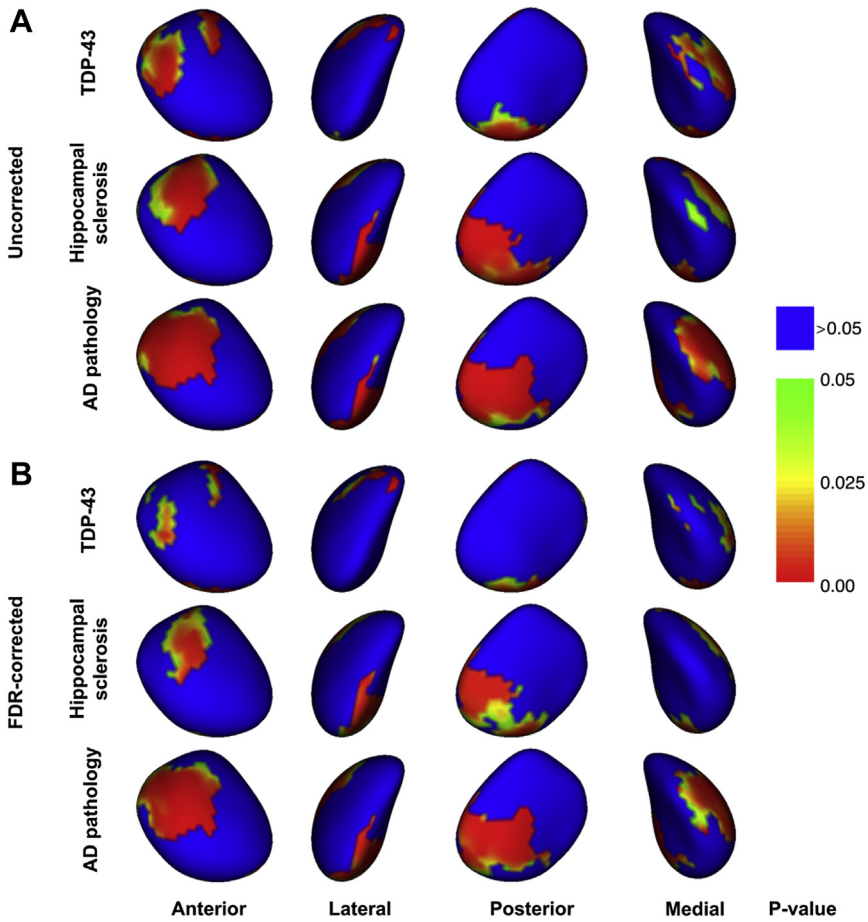

Fig. 2. (A) Uncorrected and (B) FDR-corrected significance maps demonstrating statistically significant inward deformation of the surface of the amygdala associated with TDP-43 pathology in aging, hippocampal sclerosis, and AD pathology (controlling for other neuropathologies, demographics and covariates). Red, yellow, and green colors indicate significant effects ($p < 0.05$). (For interpretation of the references to color in this figure legend, the reader is referred to the Web version of this article.)

2014). The smaller spatial extent of the laterobasal and superficial deformations associated with TDP-43 compared to those associated with AD and hippocampal sclerosis suggests that TDP-43 may be affecting fewer or smaller portions of the nuclei of these 2 subdivisions of the amygdala, implying more specialized cognitive and other clinical outcomes. In the centromedial subdivision of the amygdala inward deformation was mainly associated with TDP-43 pathology. The centromedial subdivision of the amygdala has connections to the brainstem, insula, hypothalamus, and orbital and medial prefrontal cortex (Price, 2003) and has been linked to negative emotion, fear, anger, and aggressive behavior (Caparelli et al., 2017). The presence of TDP-43 pathology in patients with AD was recently linked to agitation/aggression (Sennik et al., 2017), supporting the findings of the present work. Aggressive behavior has also been linked to AD pathology (Sennik et al., 2017), and the lack of association of centromedial amygdala deformation with AD pathology in the present work suggests that aggression in AD may be a result of frontal lobe, instead of amygdala, abnormalities. This hypothesis is further supported by the fact that aggression typically develops in later stages of AD (Sennik et al., 2017), whereas amygdala is affected early on in AD (Poulin et al., 2011).

Table 3
Association of amygdala volume with rate of change in different cognitive domains based on mixed-effects models controlling for neuropathologies and demographics[a]

	Estimate (p-value)	Percentage of variance of the rate of change explained by amygdala volume
Global cognition	$\mathbf{1.8 \cdot 10^{-4}}$ **(0.009)**	8.1%
Episodic memory	$\mathbf{1.7 \cdot 10^{-4}}$ **(0.027)**	5.3%
Semantic memory	$\mathbf{2.4 \cdot 10^{-4}}$ **(0.0012)**	8.7%
Working memory	$-6 \cdot 10^{-6}$ (0.93)	-
Perceptual speed	$\mathbf{1.8 \cdot 10^{-4}}$ **(0.029)**	3.8%
Visuospatial abilities	$8 \cdot 10^{-5}$ (0.26)	-

[a] The middle column shows the model estimates and corresponding p-values (significant estimates are shown in bold letters) for the interaction of amygdala volume with time since baseline, in mixed-effects models where the longitudinal-dependent variable was the cognitive score, and the independent variables were all the neuropathologies, demographics, amygdala volume, as well as the interaction of each one of these variables with time since baseline. The rightmost column shows the contribution of amygdala volume to the variance of the rate of change in different cognitive domains, above and beyond the contributions of neuropathologies and demographics (based on 2 mixed-effects models, with and without terms for amygdala volume and its interaction with time since baseline).

Recent studies have shown that most of older adults with hippocampal sclerosis (not related to epilepsy or acute hypoxia) also suffer by TDP-43 (Nag et al., 2015; Zarow et al., 2012). In agreement with previous reports, 92% of participants with hippocampal sclerosis were TDP-43 positive in the present work. On the other hand, many older adults with TDP-43 do not have hippocampal sclerosis (83% of TDP-43 positive participants in this work) (Nag et al., 2015). It has been suggested that persons that are TDP-43 positive but do not have hippocampal sclerosis are in an early phase of the same disease as persons that are positive to both TDP-43 and hippocampal sclerosis (Hokkanen et al., 2018). However, the exact link between TDP-43 and hippocampal sclerosis has not yet been established, and therefore, in the present work, the 2 pathologies were considered separately. In contrast, participants with

hippocampal sclerosis that were TDP-43 negative (a total of 2 persons) are not thought to be suffering by the same disease as those positive to only TDP-43 or both TDP-43 and hippocampal sclerosis. Those persons were excluded and the analysis was repeated, but the results remained essentially unchanged.

Amygdala volume explained an additional 8.1% of the variance of the rate of decline in global cognition, 5.3% in episodic memory, 8.7% in semantic memory, and 3.8% in perceptual speed, above and beyond what was explained by neuropathologies and demographics. The additional portion of the variance of the rate of cognitive decline explained by amygdala volume was substantial and indicates that this metric captures additional decline-related structural differences across participants. These structural differences may be because of: a) known pathology types that were not measured fully, b) unknown pathology that was not assessed (Nelson et al., 2018), or c) environmental or experiential factors (Maguire et al., 2000).

The findings of the present work based on ex vivo MRI are expected to translate well to the in vivo case, based on previous work using the same methodology (Dawe et al., 2011; Kotrotsou et al., 2015, 2014). More specifically, it has been shown that, for the experimental approach used here, a linear relationship exists between structural brain information collected ex vivo and in vivo on the same individuals (Kotrotsou et al., 2014). Furthermore, there is good agreement in several volumetric and shape analysis findings between previously published studies that used the same ex vivo MRI methodology and in vivo work (Dawe et al., 2011; Kotrotsou et al., 2015).

One limitation of the current investigation is that, because imaging was conducted ex vivo, the intracranial volume was not available. However, the height of the participants was used for normalization in the volumetric and shape analysis, which has previously been used as a surrogate for total intracranial volume. Also, laterality was not considered because only one hemisphere from each participant was studied, and left and right amygdalas were combined (after mirroring) in the analyses to maximize the degrees of freedom. In addition, only the score for TDP-43 pathology included measurements in the amygdala, among other regions, whereas the scores for the other pathologies were based on measurements in other predefined brain regions, following the established protocol of the parent studies (MAP, ROS), which has been presented in a number of publications. Measuring all pathologies in the amygdala is a goal of future studies. Another limitation is that, because the amygdala degenerates simultaneously with other brain regions that were not considered here, and given the fact that amygdala is mainly involved in behavior and emotion and has a lesser role in cognition, the additional portion of the variance of the rate of cognitive decline explained in this work may not be specific to the amygdala. Finally, the imaging voxels were not cubic. However, the voxel volume was 0.5 mm^3, which is smaller than that of most investigations of amygdala structure.

The present work demonstrated that TDP-43 pathology in aging not only has a significant independent negative association with the volume of the amygdala after correcting for the effects of other neuropathologies, but is also associated with a unique spatial pattern of inward deformation of the amygdala surface that is different than the patterns linked to AD pathology and hippocampal sclerosis. These findings may enhance future MR-based biomarkers. Finally, the volume of the amygdala was shown to capture additional structural contributions to the variance of the rate of cognitive decline, above and beyond what was captured by neuropathologies and demographics, suggesting that ex vivo MRI may play an important role in enhancing our understanding of cognitive aging.

Disclosure

The authors have no financial interests or relationships to disclose with regard to the subject matter of this article.

Acknowledgements

The authors would like to thank the participants and staff of the Rush Memory and Aging Project and the Religious Orders Study. The study was supported by NIH, United States grants P30AG010161, UH2NS100599, R01AG042210, R01AG17917, R01AG34374, and the Illinois Department of Public Health, United States (Alzheimer's Disease Research Fund).

References

Amunts, K., Kedo, O., Kindler, M., Pieperhoff, P., Mohlberg, H., Shah, N.J., Habel, U., Schneider, F., Zilles, K., 2005. Cytoarchitectonic mapping of the human amygdala, hippocampal region and entorhinal cortex: intersubject variability and probability maps. Anat. Embryol. (Berl). 210, 343–352.

Arai, T., Mackenzie, I.R.A., Hasegawa, M., Nonoka, T., Niizato, K., Tsuchiya, K., Iritani, S., Onaya, M., Akiyama, H., 2009. Phosphorylated TDP-43 in Alzheimer's disease and dementia with Lewy bodies. Acta. Neuropathol. 117, 125–136.

Arnold, S.J., Dugger, B.N., Beach, T.G., 2013. TDP-43 deposition in prospectively followed, cognitively normal elderly individuals: correlation with argyrophilic grains but not other concomitant pathologies. Acta. Neuropathol. 126, 51–57.

Arvanitakis, Z., Leurgans, S.E., Barnes, L.L., Bennett, D.A., Schneider, J.A., 2011a. Microinfarct pathology, dementia, and cognitive systems. Stroke 42, 722–727.

Arvanitakis, Z., Leurgans, S.E., Wang, Z., Wilson, R.S., Bennett, D.A., Schneider, J.A., 2011b. Cerebral amyloid angiopathy pathology and cognitive domains in older persons. Ann. Neurol. 69, 320–327.

Benjamini, Y., Hochberg, Y., 1995. Controlling the false discovery rate: a practical and powerful approach to multiple testing. J. R. Stat. Soc. B. 289–300.

Bennett, D.A., Buchman, A.S., Boyle, P.A., Barnes, L.L., Wilson, R.S., Schneider, J.A., 2018. Religious orders study and Rush memory and aging project. J. Alzheimers. Dis. 64, S161–S189.

Bennett, D.A., Schneider, J.A., Aggarwal, N.T., Arvanitakis, Z., Shah, R.C., Kelly, J.F., Fox, J.H., Cochran, E.J., Arends, D., Treinkman, A.D., Wilson, R.S., 2006. Decision rules guiding the clinical diagnosis of Alzheimer's disease in two community-based cohort studies compared to standard practice in a clinic-based cohort study. Neuroepidemiology 27, 169–176.

Bennett, D.A., Wilson, R.S., Schneider, J.A., Evans, D.A., Beckett, L.A., Aggarwal, N.T., Barnes, L.L., Fox, J.H., Bach, J., 2002. Natural history of mild cognitive impairment in older persons. Neurology 59, 198–205.

Boyle, P.A., Wilson, R.S., Aggarwal, N.T., Tang, Y., Bennett, D.A., 2006. Mild cognitive impairment: risk of Alzheimer disease and rate of cognitive decline. Neurology 67, 441–445.

Caparelli, E.C., Ross, T.J., Gu, H., Liang, X., Stein, E.A., Yang, Y., 2017. Graph theory reveals amygdala modules consistent with its anatomical subdivisions. Sci. Rep. 7, 14392.

Cavedo, E., Boccardi, M., Ganzola, R., Canu, E., Beltramello, A., Caltagirone, C., Thompson, P.M., Frisoni, G.B., 2011. Local amygdala structural differences with 3T MRI in patients with Alzheimer disease. Neurology 76, 727–733.

Davidson, Y.S., Raby, S., Foulds, P.G., Robinson, A., Thompson, J.C., Sikkink, S., Yusuf, I., Amin, H., Duplessis, D., Troakes, C., Al-Sarraj, S., Sloan, C., Esiri, M.M., Prasher, V.P., Allsop, D., Neary, D., Pickering-Brown, S.M., Snowden, J.S., Mann, D.M.A., 2011. TDP-43 pathological changes in early onset familial and sporadic Alzheimer's disease, late onset Alzheimer's disease and Down's Syndrome: association with age, hippocampal sclerosis and clinical phenotype. Acta. Neuropathol. 122, 703–713.

Dawe, R.J., Bennett, D.A., Schneider, J.A., Arfanakis, K., 2011. Neuropathologic correlates of hippocampal atrophy in the elderly: a clinical, pathologic, postmortem MRI study. PLoS. One. 6, e26286.

Dawe, R.J., Bennett, D.A., Schneider, J.A., Leurgans, S.E., Kotrotsou, A., Boyle, P.A., Arfanakis, K., 2014. Ex vivo T2 relaxation: associations with age-related neuropathology and cognition. Neurobiol. Aging. 35, 1549–1561.

Doty, R.L., 2017. Olfactory dysfunction in neurodegenerative diseases: is there a common pathological substrate? Lancet. Neurol. 16, 478–488.

Freeman, S.H., Spires-Jones, T., Hyman, B.T., Growdon, J.H., Frosch, M.P., 2008. TAR-DNA binding protein 43 in Pick disease. J. Neuropathol. Exp. Neurol. 67, 62–67.

Fujishiro, H., Uchikado, H., Arai, T., Hasegawa, M., Akiyama, H., Yokota, O., Tsuchiya, K., Togo, T., Iseki, E., Hirayasu, Y., 2009. Accumulation of phosphorylated TDP-43 in brains of patients with argyrophilic grain disease. Acta. Neuropathol. 117, 151–158.

Geser, F., Robinson, J.L., Malunda, J.A., Xie, S.X., Clark, C.M., Kwong, L.K., Moberg, P.J., Moore, E.M., Van Deerlin, V.M., Lee, V.M.-Y., Arnold, S.E., Trojanowski, J.Q., 2010. Pathological 43-kDa transactivation response DNA-binding protein in older adults with and without severe Mental illness. Arch. Neurol. 67, 1238–1250.

Geser, F., Winton, M.J., Kwong, L.K., Xu, Y., Xie, S.X., Igaz, L.M., Garruto, R.M., Perl, D.P., Galasko, D., Lee, V.M., Trojanowski, J.Q., 2008. Pathological TDP-43 in parkinsonism-dementia complex and amyotrophic lateral sclerosis of Guam. Acta. Neuropathol. 115, 133–145.

Hokkanen, S.R.K., Hunter, S., Polvikoski, T.M., Keage, H.A.D., Minett, T., Matthews, F.E., Brayne, C., 2018. Hippocampal sclerosis, hippocampal neuron loss patterns TDP-43 aged population. Brain. Pathol. 28, 548–559.

James, B.D., Wilson, R.S., Boyle, P.A., Trojanowski, J.Q., Bennett, D.A., Schneider, J.A., 2016. TDP-43 stage, mixed pathologies, and clinical Alzheimer's-type dementia. Brain 139, 2983–2993.
Josephs, K.A., 2010. Dementia and the TAR DNA binding protein 43. Clin. Pharmacol. Ther. 88, 555–558.
Josephs, K.A., Dickson, D.W., 2016. TDP-43 in the olfactory bulb in Alzheimer's disease. Neuropathol. Appl. Neurobiol. 42, 390–393.
Josephs, K.A., Murray, M.E., Whitwell, J.L., Parisi, J.E., Petrucelli, L., Jack, C.R., Petersen, R.C., Dickson, D.W., 2014a. Staging TDP-43 pathology in Alzheimer's disease. Acta. Neuropathol. 127, 441–450.
Josephs, K.A., Whitwell, J.L., Weigand, S.D., Murray, M.E., Tosakulwong, N., Liesinger, A.M., Petrucelli, L., Senjem, M.L., Knopman, D.S., Boeve, B.F., Ivnik, R.J., Smith, G.E., Jack, C.R., Parisi, J.E., Petersen, R.C., Dickson, D.W., 2014b. TDP-43 is a key player in the clinical features associated with Alzheimer's disease. Acta. Neuropathol. 127, 811–824.
Koga, S., Sanchez-Contreras, M., Josephs, K.A., Uitti, R.J., Graff-Radford, N., van Gerpen, J.A., Cheshire, W.P., Wszolek, Z.K., Rademakers, R., Dickson, D.W., 2016. Distribution and characteristics of transactive response DNA binding protein 43 kDa pathology in progressive supranuclear palsy. Mov. Disord. 32, 246–255.
Kotrotsou, A., Bennett, D.A., Schneider, J.A., Dawe, R.J., Golak, T., Leurgans, S.E., Yu, L., Arfanakis, K., 2014. Ex vivo MR volumetry of human brain hemispheres. Magn. Reson. Med. 71, 364–374.
Kotrotsou, A., Schneider, J.A., Bennett, D.A., Leurgans, S.E., Dawe, R.J., Boyle, P.A., Golak, T., Arfanakis, K., 2015. Neuropathologic correlates of regional brain volumes in a community cohort of older adults. Neurobiol. Aging. 36, 2798–2805.
Kromer Vogt, L.J., Hyman, B.T., Van Hoesen, G.W., Damasio, A.R., 1990. Pathological alterations in the amygdala in Alzheimer's disease. Neuroscience 37, 377–385.
LeDoux, J.E., Schiller, D., 2009. What animal fear models have taught us about human amygdala function? In: Whalen, P.J., Phelps, E.A. (Eds.), The Human Amygdala. Guilford Press, New York, NY, pp. 43–60.
Lippa, C.F., Rosso, A.L., Stutzbach, L.D., Neumann, M., Lee, V.M., Trojanowski, J.Q., 2010. Transactive response DNA-binding protein 43 burden in familial Alzheimer disease and Down syndrome. Arch. Neurol. 66, 1483–1488.
Maguire, E.A., Gadian, D.G., Johnsrude, I.S., Good, C.D., Ashburner, J., Frackowiak, R.S., Frith, C.D., 2000. Navigation-related structural change in the hippocampi of taxi drivers. Proc. Natl. Acad. Sci. U S A 97, 4398–4403.
Mcaleese, K.E., Walker, L., Erskine, D., Thomas, A.J., Mckeith, I.G., Attems, J., 2016. TDP-43 pathology in Alzheimer's disease, dementia with Lewy bodies and ageing. Brain. Pathol. 27, 472–479.
McKeith, I.G., Galasko, D., Kosaka, K., Perry, E.K., Dickson, D.W., Hansen, L.A., Salmon, D.P., Lowe, J., Mirra, S.S., Byrne, E.J., Lennox, G., Quinn, N.P., Edwardson, J.A., Ince, P.G., Bergeron, C., Burns, A., Miller, B.L., Lovestone, S., Collerton, D., Jansen, E.N.H., Ballard, C., de Vos, R.A.I., Wilcock, G.K., Jellinger, K.A., Perry, R.H., 1996. Consensus guidelines for the clinical and pathologic diagnosis of dementia with Lewy bodies (DLB). Neurology 47, 1113–1124.
McKhann, G., Drachman, D., Folstein, M., Katzman, R., Price, D., Stadlan, E.M., 1984. Clinical diagnosis of Alzheimer's disease: report of the NINCDS-ADRDA work group under the auspices of department of Health and human services task force on Alzheimer's disease. Neurology 34, 939–944.
Miller, M.I., Younes, L., Ratnanather, J.T., Brown, T., Trinh, H., Lee, D.S., Tward, D., Mahon, P.B., Mori, S., Albert, M., 2015. Amygdalar atrophy in symptomatic Alzheimer's disease based on diffeomorphometry: the BIOCARD cohort. Neurobiol. Aging. 36, S3–S10.
Nag, S., Yu, L., Boyle, P.A., Leurgans, S.E., Bennett, D.A., Schneider, J.A., 2018. TDP-43 pathology in anterior temporal pole cortex in aging and Alzheimer's disease. Acta. Neuropathol. Commun. 6, 33.
Nag, S., Yu, L., Capuano, A.W., Wilson, R.S., Leurgans, S.E., Bennett, D.A., Schneider, J.A., 2015. Hippocampal sclerosis and TDP-43 pathology in aging and Alzheimer disease. Ann. Neurol. 77, 942–952.
Nelson, P.T., Abner, E.L., Patel, E., Anderson, S., Wilcock, D.M., Kryscio, R.J., Van Eldik, L.J., Jicha, G.A., Gal, Z., Nelson, R.S., Nelson, B.G., Gal, J., Azam, M.T., Fardo, D.W., Cykowski, M.D., 2018. The amygdala as a locus of pathologic Misfolding in neurodegenerative diseases. J. Neuropathol. Exp. Neurol. 77, 2–20.
Nelson, P.T., Abner, E.L., Schmitt, F.A., Kryscio, R.J., Jicha, G.A., Smith, C.D., Davis, D.G., Poduska, J.W., Patel, E., Mendiondo, M.S., Markesbery, W.R., 2010. Modeling the association between 43 different clinical and pathological variables and the severity of cognitive impairment in a large autopsy cohort of elderly persons. Brain. Pathol. 20, 66–79.
Neumann, M., Sampathu, D.M., Kwong, L.K., Truax, A.C., Micsenyi, M.C., Chou, T.T., Bruce, J., Schuck, T., Grossman, M., Clark, C.M., McCluskey, L.F., Miller, B.L., Masliah, E., Mackenzie, I.R., Feldman, H., Feiden, W., Kretzschmar, H.A., Trojanowski, J.Q., Lee, V.M., 2006. Ubiquitinated TDP-43 in frontotemporal lobar degeneration and amyotrophic lateral sclerosis. Science 314, 130–133.
Olivé, M., Janué, A., Moreno, D., Gámez, J., Torrejón-Escribano, B., Ferrer, I., 2009. TAR DNA-Binding protein 43 accumulation in protein aggregate myopathies. J. Neuropathol. Exp. Neurol. 68, 262–273.
Pikkarainen, M., Rönkkö, S., Savander, V., Insausti, R., Pitkänen, A., 1999. Projections from the lateral, basal, and accessory basal nuclei of the amygdala to the hippocampal formation in rat. J. Comp. Neurol. 403, 229–260.
Pitkänen, A., Kelly, J.L., Amaral, D.G., 2002. Projections from the lateral, basal, and accessory basal nuclei of the amygdala to the entorhinal cortex in the macaque monkey. Hippocampus 12, 186–205.
Poulin, S.P., Dautoff, R., Morris, J.C., Barrett, L.F., Dickerson, B.C., Alzheimer's Disease Neuroimaging Initiative, 2011. Amygdala atrophy is prominent in early Alzheimer's disease and relates to symptom severity. Psychiatry. Res. 194, 7–13.
Price, J.L., 2003. Comparative aspects of amygdala connectivity. Ann. N. Y. Acad. Sci. 985, 50–58.
Qiu, A., Fennema-Notestine, C., Dale, A.M., Miller, M.I., 2009. Regional shape abnormalities in mild cognitive impairment and Alzheimer's disease. Neuroimage 45, 656–661.
Schneider, J.A., Arvanitakis, Z., Leurgans, S.E., Bennett, D.A., 2009. The neuropathology of probable Alzheimer disease and mild cognitive impairment. Ann. Neurol. 66, 200–208.
Schneider, J.A., Arvanitakis, Z., Yu, L., Boyle, P.A., Leurgans, S.E., Bennett, D.A., 2012. Cognitive impairment, decline and fluctuations in older community-dwelling subjects with Lewy bodies. Brain 135, 3005–3014.
Schneider, J.A., Boyle, P.A., Arvanitakis, Z., Bienias, J.L., Bennett, D.A., 2007. Subcortical infarcts, Alzheimer's disease pathology, and memory function in older persons. Ann. Neurol. 62, 59–66.
Schwab, C., Arai, T., Hasegawa, M., Akiyama, H., Yu, S., McGeer, P.L., 2009. TDP-43 pathology in familial British dementia. Acta. Neuropathol. 118, 303–311.
Schwab, C., Arai, T., Hasegawa, M., Yu, S., Mcgeer, P.L., 2008. Colocalization of transactivation-responsive DNA-binding protein 43 and huntingtin in inclusions of huntington disease. J. Neuropathol. Exp. Neurol. 67, 1159–1165.
Sennik, S., Schweizer, T.A., Fischer, C.E., Munoz, D.G., 2017. Risk factors and pathological substrates associated with agitation/aggression in Alzheimer's disease: a preliminary study using NACC data. J. Alzheimers. Dis. 55, 1519–1528.
Smith, S.M., Jenkinson, M., Woolrich, M.W., Beckmann, C.F., Behrens, T.E.J., Johansen-Berg, H., Bannister, P.R., De Luca, M., Drobnjak, I., Flitney, D.E., Niazy, R.K., Saunders, J., Vickers, J., Zhang, Y., De Stefano, N., Brady, J.M., Matthews, P.M., 2004. Advances in functional and structural MR image analysis and implementation as FSL. Neuroimage 23 (Suppl 1), S208–S219.
Styner, M., Oguz, I., Xu, S., Brechbühler, C., Pantazis, D., Levitt, J.J., Shenton, M.E., Gerig, G., 2006. Framework for the statistical shape analysis of brain structures using SPHARM-PDM. Insight. J. 242–250.
Styner, M.A., Rajamani, K.T., Nolte, L.-P., Zsemlye, G., Székely, G., Taylor, C.J., Davies, R.H., 2003. Evaluation of 3D correspondence methods for model building. Inf. Process. Med. Imaging. 18, 63–75.
Takeda, T., Uchihara, T., Kawamura, S., Ohashi, T., 2014. Olfactory dysfunction related to TDP-43 pathology in amyotrophic lateral sclerosis. Clin. Neuropathol. 33, 65–67.
Tang, X., Holland, D., Dale, A.M., Younes, L., Miller, M.I., 2015. The diffeomorphometry of regional shape change rates and its relevance to cognitive deterioration in mild cognitive impairment and Alzheimer's disease. Hum. Brain. Mapp. 36, 2093–2117.
Tang, X., Holland, D., Dale, A.M., Younes, L., Miller, M.I., 2014. Shape abnormalities of subcortical and ventricular structures in mild cognitive impairment and Alzheimer's disease: detecting, quantifying, and predicting. Hum. Brain. Mapp. 35, 3701–3725.
Tang, X., Varma, V.R., Miller, M.I., Carlson, M.C., 2017. Education is associated with sub-regions of the hippocampus and the amygdala vulnerable to neuropathologies of Alzheimer's disease. Brain. Struct. Funct. 222, 1469–1479.
Tremblay, C., St-Amour, I., Schneider, J., Bennett, D.A., Calon, F., 2011. Accumulation of transactive response DNA binding protein 43 in mild cognitive impairment and Alzheimer disease **. J. Neuropathol. Exp. Neurol. 70, 788–798.
Uchino, A., Takao, M., Hatsuta, H., Sumikura, H., Nakano, Y., Nogami, A., Saito, Y., Arai, T., Nishiyama, K., Murayama, S., 2015. Incidence and extent of TDP-43 accumulation in aging human brain. Acta. Neuropathol. Commun. 3, 35.
Uryu, K., Nakashima-Yasuda, H., Forman, M.S., Kwong, L.K., Clark, C.M., Grossman, M., Miller, B.L., Kretzschmar, H.A., Lee, V.M., Trojanowski, J.Q., Neumann, M., 2013. Concomitant TAR-DNA-binding protein 43 pathology is present in Alzheimer disease and corticobasal degeneration but not in other tauopathies. J. Neuropathol. Exp. Neurol. 67, 555–564.
Van Petten, C., 2004. Relationship between hippocampal volume and memory ability in healthy individuals across the lifespan: review and meta-analysis. Neuropsychologia 42, 1394–1413.
Wider, C., Dickson, D.W., Stoessl, A.J., Tsuboi, Y., Chapon, F., Gutmann, L., Lechevalier, B., Calne, D.B., Personett, D.A., Hulihan, M., Kachergus, J., Rademakers, R., Baker, M.C., Grantier, L.L., Sujith, O.K., Brown, L., Calne, S., Farrer, M.J., Wszolek, Z.K., 2009. Pallidonigral TDP-43 pathology in Perry syndrome. Parkinsonism. Relat. Disord. 15, 281–286.
Wilson, R., Barnes, L., Bennett, D., 2003. Assessment of lifetime participation in cognitively stimulating activities. J. Clin. Exp. Neuropsychol. 25, 634–642.
Wilson, R.S., Yu, L., Trojanowski, J.Q., Chen, E.Y., Boyle, P.A., Bennett, D.A., Schneider, J.A., 2013. TDP-43 pathology, cognitive decline, and dementia in old age. JAMA. Neurol. 70, 1418–1424.
Yokota, O., Davidson, Y., Arai, T., Hasegawa, M., Akiyama, H., Ishizu, H., Terada, S., Sikkink, S., Pickering-Brown, S., Mann, D.M.A., 2010. Effect of topographical distribution of α-synuclein pathology on TDP-43 accumulation in Lewy body disease. Acta. Neuropathol. 120, 789–801.
Yu, L., De Jager, P.L., Yang, J., Trojanowski, J.Q., Bennett, D.A., Schneider, J.A., 2015. The TMEM106B locus and TDP-43 pathology in older persons without FTLD. Neurology 84, 927–934.
Zarow, C., Weiner, M.W., Ellis, W.G., Chui, H.C., 2012. Prevalence, laterality, and comorbidity of hippocampal sclerosis in an autopsy sample. Brain. Behav. 2, 435–442.